# Integration Framework for Improved Visual Servoing in Image and Cartesian Spaces

A. H. Abdul Hafez
Dept. of Computer Science and Engineering
University College of Engineering, Osmania University
Hyderabad-500007, India
Email: hafezsyr@ieee.org

C. V. Jawahar
Center for Visual Information Technology
International Institute of Information Technology
Gachibowli, Hyderabad-500032, India
Email: jawahar@iiit.ac.in

***Abstract*— In this paper, we present a new integration method for improving the performance of visual servoing. The method integrates both image-based visual servoing (IBVS) and position-based visual servoing (PBVS) to satisfy the requirements of the visual servoing process. We define a probabilistic integration rule for IBVS and PBVS controllers. Density functions that determine the probability of each controller are defined to satisfy the above constraints. We prove that this integration method provides global stability, and avoids local minima. The new integration method is validated on positioning tasks, and compared with other switching methods.**

## I. Introduction

Visual servoing is a method in which visual feedback is introduced in the robot control loop to increase the accuracy of the overall robot system. This saves the need to increase the accuracy of different parts like end-effector and sensors attached to the system. In addition, visual feedback helps in controlling the robot pose with respect to a target even in the presence of calibration errors. Visual servoing has become an attractive area of research and has recently received considerable amount of attention [1], [2], [3].

Visual servoing techniques are divided into three classes. These classes are: image-based, position-based, and hybrid visual servoing. These divisions are respectively based on the use of 2D information from the image space, 3D information from the Cartesian space, or a mixture of both kinds of information. While image-based visual servoing and position-based visual servoing have complementary advantages and disadvantages, hybrid methods attempt to incorporate the advantages of both methods.

Maintaining visibility of features, local minima avoidance, preference for shortest path, and avoidance of image singularity are some of the challenges faced in the field of visual servoing [4], [5]. In this paper, we present a probabilistic framework that integrates the classical architectures, IBVS and PBVS into one architecture. The integration process uses weights to determine the relative importance of each sub-controller. These weights are computed through probability density functions which are designed to satisfy the above challenges.

## II. Related Work and Problem Formulation

Recent research in the visual servoing field has concentrated on development of algorithms which satisfy one or more of the requirements mentioned in Section I. The most comprehensive solutions are based on potential fields [3], [6], [5], which was originally introduced to the robotic community by Khatib in [7] as a solution to the collision avoidance problem. Most of the earlier works tried to address the visibility problem without any attention toward the local minima and Cartesian camera trajectory. The method presented in [5] solved the local minima problem, but the camera path is neither straight line nor smooth.

Mesouar and Chaumette [6] have recently proposed a potential field based method for path planning in the image space. This method introduces the visibility and robot joint limits constraints into the design of the desired trajectories. Essentially, this is a local path planning method where the local minima is not ensured to be avoidable when repulsive and attractive fields are equal. In addition, the camera trajectory is not predictable when the repulsive forces are involved.

Gans and Hutchinson [8] have proposed a switching approach between IBVS and PBVS. The proposed controller consists of two sub-controllers for IBVS and PBVS. Whenever the features are going to get out of the field of view (FoV) of the camera, the control switches to IBVS, and whenever the camera starts retreat, the control switches back to PBVS. However, the global stability is not ensured in this scheme. The binary switching allows either IBVS or PBVS controller to work at a specific instance. They did not consider the potential local minima, which was demonstrated in [4], neither in the image space nor in the Cartesian space. In addition, a discontinuity in the velocity control signal can be observed at the time of switching between the two sub-controllers. This algorithm also needs more time to converge. The reason behind this is that switching from IBVS to PBVS may increase the image error, which is minimized using the IBVS controller.

In Chesi *et. al.* [9], a switching approach between elementary camera movements is proposed. A sequence of high level if-then-else rules is used to switch between camera rotation, translation, or backward translation along the camera optical axis. This method, shows a discontinuity in the velocity control signal in addition to longer time of convergence owing to the switching time to keep features in the FoV. The Cartesian local minima due to errors in homography estimation is not considered. In addition, the camera trajectory is not straight

line any more because of the backward translation.

The method proposed in this paper is based on a probabilistic integration scheme. It outperforms the reported methods available in the literature. Experimental results validate our claim.

## III. Probabilistic Integration Framework

Let $\mathcal{V} = \{V_i\}$, where $\mathcal{V} \subseteq R^6$ be a set of possible states of the velocity screw vector commanded to the robot arm controller. The probability that the velocity vector $V$ uses the value $V_i$ conditioned to the image measurements vector $x$ is

$$p(V = V_i|x) = p(V_i|x). \tag{1}$$

By convention, these probabilities sum to unity $\int_{\mathcal{V}} p(V_i|x) = 1$. The conditioned expected value of the velocity vector over the universe $\mathcal{V}$ is

$$\hat{V} = E(V_i|x) = \int_{\mathcal{V}} V_i \; p(V_i|x) \; dV_i. \tag{2}$$

Let us define another parameter $\alpha_i$ of the visual servoing process. Consider that we have $N$ individual visual servoing control laws represented by the parameters $\alpha_i$. For example, an integration can be done between IBVS and PBVS control laws, then $i$ takes the values $\{im, po\}$. In case of using an integration between rotation, translation, and backward translation control laws from a given scheme, then $i$ takes the values $\{ro, tr, ba\}$.

It is possible to rewrite the probability function $p(V_i|x)$ as

$$p(V_i|x) = \int_{\alpha} p(V_i, \alpha|x) \; d\alpha = \int_{\alpha} p(V_i|\alpha, x) \; p(\alpha|x) \; d\alpha. \tag{3}$$

By substituting (3) in (2), the conditional mean of the velocity can be rewritten after some developments as

$$\hat{V} = \int_{\alpha} p(\alpha|x) \; \hat{V}(\alpha) \; d\alpha, \tag{4}$$

where, $\hat{V}(\alpha) = \int_{\mathcal{V}} V_i \; p(V_i|\alpha, x) \; dV_i$, and in the discrete case

$$\hat{V} = \sum_{\alpha_i} \hat{V}(\alpha_i) \; p(\alpha_i|x), \quad \text{where} \; \sum_{\alpha_i} p(\alpha_i|x) = 1. \tag{5}$$

Here $p(\alpha_i|x)$ is the discrete probability for $\alpha_i$, conditioned on the image measurement $x$. Equation (5) says that the optimal estimate of the velocity vector is a weighted summation of the velocity values computed from each individual control law. This is shown in Fig (1). The problem is now reduced to the computation of the velocity from each individual controller in addition to the computation of the probabilities of using each of these individual controllers.

## IV. Integrated IBVS and PBVS

### A. Image-based and Position-based Visual Servoing

In Image-based visual servoing, the task function is defined with respect to the error $e(s) = s - s^*$ in the image space, where $s$ is the vector of the current features position and $s^*$ is the vector of the desired one. The velocity screw using IBVS is given as [1]

$$\dot{e_i} = J_i V_i \tag{6}$$

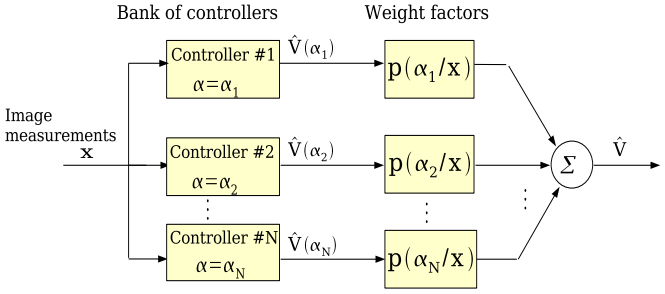


Fig. 1. Weighted sum of the velocity estimates

$$V_i = -\lambda_i J_i^+ e_i(s), \tag{7}$$

where $J_i^+$ is the pseudo-inverse of the Jacobian matrix $J_i$.

It is easy to show that the feature trajectory in the image space is a straight line while the camera trajectory in the Cartesian space is unpredictable. Indeed, from any initial state, IBVS moves the image points straight toward its desired positions in the image. This is subject to the availability of a good estimate of the depth and robust image measurements. IBVS is proved to be asymptotically locally stable, but the global stability is not ensured since unpredictable image local minima and Jacobian singularity may occurs at any time.

In position-based visual servoing, the camera velocity is defined as a function of the error between the current and desired camera pose. This error is the transformation $T_C^{C*}$ represented as a $(6 \times 1)$ vector $e_p = [t_C^{C*}, u\theta]^T$.

The velocity screw using PBVS is given as [1]

$$\dot{e_p} = J_p V_p \tag{8}$$

$$V_p = -\lambda_p J_p^{-1} e_p \tag{9}$$

where $J_p$ is the interaction matrix [10].

While PBVS minimize the error function in the Cartesian space, the camera trajectory is a straight line, but the feature trajectory is not predictable and may get out of the camera field of view. However, PBVS method is known to be globally asymptotically stable and does not suffer from any local minima or Jacobian singularity. The global stability is subject to an accurate estimate of the pose.

### B. The Integration Rule

Two individual image-based visual servoing and position-based visual servoing control laws can be integrated using (5)

$$\hat{V} = \hat{V}(\alpha_{im}) \; p(\alpha_{im}|x) + \hat{V}(\alpha_{po}) \; p(\alpha_{po}|x). \tag{10}$$

Here, $\hat{V}(\alpha_{im})$ is the velocity computed using the IBVS controller given in (7). The velocity $\hat{V}(\alpha_{po})$ is computed using the PBVS controller given in (9). The probability of using each individual control law $p(\alpha_i|x)$, conditioned on the image measurement $x$, is determined by the image and Cartesian constraints to be satisfied during the process of visual servoing. The probabilistic weights $p(\alpha_{im}|x)$ and $p(\alpha_{po}|x)$ given in (10) can be normalized in such a way that it sums upto one, to

satisfy (5). Replacing the normalized term $\frac{p(\alpha_{im}|x)}{p(\alpha_{im}|x)+p(\alpha_{po}|x)}$ by $\omega$ and $\frac{p(\alpha_{po}|x)}{p(\alpha_{im}|x)+p(\alpha_{po}|x)}$ by $(1-\omega)$ gives

$$\hat{V} = \omega\hat{V}(\alpha_{im}) + (1-\omega)\hat{V}(\alpha_{po}), \text{ where } 0 < \omega < 1. \quad (11)$$

The probability $p(\alpha_{po}|x)$ will be defined as

$$p(\alpha_{po}|x) \;=\; p_s(\alpha_{po}|x)p_l(\alpha_{po}|x),$$

where the subscripts $l$ and $s$ indicate to local minima and straight camera trajectory respectively. The fact that PBVS is preferable to produce a straight camera trajectory whenever the features visibility and local minima constraints are satisfied is interpreted as $p_s(\alpha_{po}|x) = 1$.

To account for Cartesian local minima that may exist owing to errors in pose estimation process, the probability $p(\alpha_{im}|x)$ should also increases near to it. In this way, the probability $p(\alpha_{im}|x)$ is divided to be the multiplication of two terms as following

$$p(\alpha_{im}|x) = p_v(\alpha_{im}|x)p_l(\alpha_{im}|x),$$

where $p_v(\alpha_{im}|x)$ corresponds to the features visibility and $p_l(\alpha_{im}|x)$ corresponds to the Cartesian local minima.

Note that this framework is a superior generic framework of the switching methods proposed either in [8] or in [9]. The difference between the proposed and these two methods is that $\omega \in \{0, 1\}$, while $\alpha_i \in \{\alpha_{im}, \alpha_{po}\}$ in [8] and $\alpha_i \in \{\alpha_{ro}, \alpha_{tr}, \alpha_{ba}\}$ in [9]. In our method, $0 < \omega < 1$.

### C. Feature-visibility

If the initial and desired positions of the image points are well chosen in such a way that all features are in the camera field of view, the image points are ensured to be in the FoV during the whole process. The probability of using image-based visual servoing $\omega$, conditioned on the image measurement $x$, increases when one of the image points approaches the image boundary more than a threshold $D_0$.

Given $N$ image points as features, let us define the vector $D$ where its element $d_i$ is the distance vector of the $i$th point to the nearest image boundary. The probability $\omega$ should increase when $d_{min}$ is decreasing, where $d_{min}$ is given as $d_{min} = \min_{d_i}(D)$. ¿From the discussion above, the probability function $p_v(\alpha_{im}|x)$ can be formulated as the following normal density function

$$p_v(\alpha_{im}|x) = \mathcal{N}(d_{min}; D_0, \sigma_D), \quad (12)$$

where $\sigma_D$ is the variance and its value is selected depends on the image size and the threshold $D_0$.

### D. Image and Cartesian Local Minima

The evaluation of Cartesian local minima is done in terms of the energy function in the space of 3D pose error $\mathcal{E}_p = \frac{1}{2}e_p^T e_p$, and its gradient vector $G_p(t)$ with respect to time $t$. At every time instant $t$, the gradient vector $G_p(t)$ is given as

$$G_p(t,s) = \frac{\partial \mathcal{E}_p}{\partial t}\Big|_{t,s} = (e_p)^T \frac{\partial e_p}{\partial t} = (e_p)^T J_p \hat{V}(\alpha_{po}), \quad (13)$$

where $J_p$ is the pose Jacobian. Cartesian local minima occurs when the value of the norm of the gradient vector $\hat{G}_p(t)$ is going to be smaller than a threshold value $G_{0p}$. Indeed, the probability density function of Cartesian local minima is formulated as following

$$p_l(\alpha_{im}|x) = \mathcal{N}(\hat{G}_p(t); G_{0p}, \sigma_{Gp}), \quad (14)$$

where $\hat{G}_p(t)$ is the norm of the vector $G_p(t)$, and $\sigma_{Gp} = \frac{\mathcal{E}_p(0)}{\rho}$ is the variance. Here, $\mathcal{E}_p(0)$ is the pose space energy function at the initial stage $t = 0$, and $\epsilon$ is a positive scalar, its value is selected to avoid nullifying $p(\alpha_{im}|x)$ if there is no desired image feature that is near to the image border.

The evaluation of image local minima is done in terms of the energy function in the image space $\mathcal{E}_i = \frac{1}{2}e_i^T e_i$, and its gradient vector $G_i(t)$ with respect to time $t$. At every time instant $t$, the gradient vector $G_i(t)$ is given as

$$G_i(t,s) = \frac{\partial \mathcal{E}_i}{\partial t}\Big|_{t,s} = (s_t - s_d)^T \frac{\partial s_t}{\partial t} = (s_t - s_d)^T J_i \hat{V}, \quad (15)$$

where $J_i$ is the image Jacobian. Image local minima occurs when the norm of the gradient vector $\hat{G}_i(t)$ is near the zero. Therefor, the probability $\omega$ should decrease at or near to the image local minima. Indeed, the probability density function of image local minima is formulated as following

$$p_l(\alpha_{po}|x) = \eta\, \mathcal{N}(\hat{G}_i(t); G_{0i}, \sigma_{Gi}), + \mu \quad (16)$$

where $\hat{G}_i(t)$ is the norm of the vector $G_i(t)$, and $\sigma_{Gi}$ is the variance. The constants $\eta$ and $\mu$ are selected depends on the state of the energy function $\mathcal{E}_i$ with respect to the global minima at the desired state as following:

$$\begin{cases} \eta = 1,\ \mu = 0.387, & \text{if } \mathcal{E}_i > \rho; \\ \eta = 0,\ \mu = 0.01, & \text{if } \mathcal{E}_i \leq \rho. \end{cases} \quad (17)$$

Here, $\rho$ defines a convergence neighborhood around the desired feature position. Defining $p_l(\alpha_{po}|x)$ in this form is useful to distinguish between local and global image minima. In other words, the definition of the previous probabilities acts in such a way that $p(\alpha_{po}|x)$ increases only at the image local minima while it vanishes to small value at the global minima where IBVS is preferable.

## V. Stability Analysis

### A. Local Stability

Local stability is considered only in a neighborhood of the convergence (equilibrium) point. An equilibrium point is locally asymptotically stable if all solutions starting in a small neighborhood converge to the equilibrium point. stability of equilibrium point is characterized by Lyapunov function. Considering linear systems, the local and global stability are same. The necessary and sufficient condition for local/global asymptotic stability of a linear system $\dot{e} = \mathcal{A}e$ is that the matrix $\mathcal{A}$ describing the system has negative real parts for all its eigenvalues. Usually, eigenvalues with zeros or real part do not void the stability but contrarily not giving robustness

because it may shift to the positive part when the system is affected by noise or disturbance. In fact, our system is a convex combination of two linear systems; the matrices $J_i$ and $J_p$ are fixed and non-singular in a neighborhood of the equilibrium point. Stability for such a system needs to ensure that there exist a Lyapunov function for this combination.

Substituting (7) and (9) in (11), we write

$$\hat{V} = -\omega J_i^{+} e_i - (1-\omega) J_p^{-1} e_p. \tag{18}$$

Equations (6) and (8) can be concatenated and rewritten in the following equation

$$\begin{bmatrix} \dot{e_i} \\ \dot{e_p} \end{bmatrix} = \begin{bmatrix} J_i \\ J_p \end{bmatrix} \hat{V} \tag{19}$$

By rearranging (18) and substituting in (19) we get the convex combination system $\dot{e} = \mathcal{A}e$. Here,

$$\mathcal{A} = \omega A_1 + (1-\omega) A_2, \tag{20}$$

where $A_1 = \begin{bmatrix} -I_6 & 0 \\ -J_p J_i^{+} & 0 \end{bmatrix}$ and $A_2 = \begin{bmatrix} 0 & -J_i J_p^{-1} \\ 0 & -I_6 \end{bmatrix}$. The matrices $A_1$ and $A_2$ define, with the parameter $\omega$, a one parameter family of matrices in the form given in (20). This family is called [11] the matrix pencil $\gamma_\omega(A_1, A_2),\ \omega \in [0,1]$.

*Theorem 1:* The pair of linear systems given in (20) has a quadratic common Lyapunov function if and only if all the matrices in $\gamma_\omega(A_1, A_2)$ and in $\gamma_\omega(A_1, A_2^{-1})$ are stable [12].

Let us have a closer look to the matrix pencil $\mathcal{A} = \gamma_\omega(A_1, A_2)$ that is given in (20). In fact, this matrix pencil can be written as

$$\mathcal{A} = \begin{bmatrix} -\omega I_6 & -(1-\omega) J_i J_p^{-1} \\ -\omega J_p J_i^{+} & -(1-\omega) I_6 \end{bmatrix}. \tag{21}$$

One can easily note the linear dependency between the first six rows and the last six ones. This is due to the fact that the matrices in the upper right corner and lower left corner are the inverse of each other. This yields a system with six negative eigenvalues and six zero eigenvalues. However, the six zero eigenvalues are owing to the special form of the matrix $\mathcal{A}$ and will not move to the positive part when the system is affected by noise or disturbance. Consequently, we can conclude that all matrices in the matrix pencil $\mathcal{A} = \gamma_\omega(A_1, A_2)$ are stable whenever the matrices $J_i$ and $J_p$ are invertible and nonsingular. However, this is ensured in the neighborhood of the equilibrium point where these matrices $J_i$ and $J_p$ are fixed with full rank. Similarly, it can be shown that all matrices in the matrix pencil $\mathcal{A} = \gamma_\omega(A_1, A_2^{-1})$ are stable.

According to Theorem 1, $\forall\ \omega \in [0,1]$, the convex combination of the systems given in (20) is stable and there exist a quadratic common Lyapunov function. A common Lyapunov function means that there exist symmetric positive definite matrices $P$ and $Q$ such that $\mathcal{A}^T P + P\mathcal{A} = -Q$. In other words,

$$\omega\Big(A_1^T P + P A_1\Big) + (1-\omega)\Big(A_2^T P + P A_2\Big) = -Q, \tag{22}$$

$$\omega\ e^T\Big(A_1^T P + P A_1\Big)e + (1-\omega)\ e^T\Big(A_2^T P + P A_2\Big)e$$

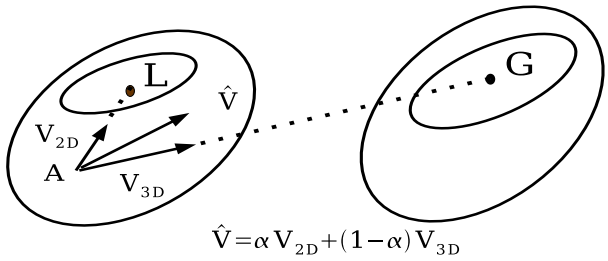


Fig. 2. Representation of the velocity vectors in 2D space.

$$= -e^T Q e < 0, \tag{23}$$

$\forall e \in R^n \backslash \{0\}$. In other words, $R^n \backslash \{0\}$ is covered by the union of the two open conic regions: (i) $\Re_1 = \{e,\ e^T(A_1^T P + P A_1)e < 0\}$, and (ii) $\Re_2 = \{e,\ e^T(A_2^T P + P A_2)e < 0\}$. Thus, the function $V(e) = e^T P e$ decreases along solutions from $A_1$ in region $\Re_1$ and along solutions from $A_2$ in region $\Re_2$. While all matrices in the matrix pencil $\gamma_\omega(A_1, A_2)$ are stable, the Lyapunov function $V(e)$ decreases along solutions for all $\omega$.

### *B. Global Stability*

It was proved in [13] that for both IBVS and PBVS, there exist a range of camera poses where under a visual servoing algorithm both image error $e_i$ and pose error $e_p$ decrease to zero. In addition, if the pose error consists of a translation and sufficiently small rotation, the system is within this region. Consequently, a pose error with a translation and sufficiently small rotation can be regulated to zero either using IBVS or PBVS.

To analyze the behaviour of the proposed integrated system in the nieghborhood of an image local minima, a 2D projection of the velocity vector is presented in Fig 2. The point A represents a current work point in the nieghborhood of an image local minima represented by the point L, while the point G represents the global minima. In the nieborhood of L, the direction of $\hat{V}(\alpha_{im})$ is toward L. Where PBVS is globally stable or at least local minima may occur in the neighborhood of the global one G, the vector $\hat{V}(\alpha_{po})$ is independent on L and always points toward the global minima G. It is clear that the weighted sum of these two vectors $\hat{V}(\alpha_{im})$ and $\hat{V}(\alpha_{po})$ will drive the system away from the local minima L toward the global minima G. After a few iterations, the system escape from the local minima by getting out of its neighborhood. Regardless the rotation error has been increased or decreased in the neighborhood of the local minima it will start decreasing again after escaping it up to the reaching the stability region. In the stability region *i.e.* the neighborhood of the global minima, both image error and pose error decrease monotonically to the global minima.

We argue that the rotation part in the pose error decreases to small value in spite of the existence of an image local minima. This allows the translation part to start decreasing when the rotation error becomes sufficiently small. Because $0 < \omega < 1$,

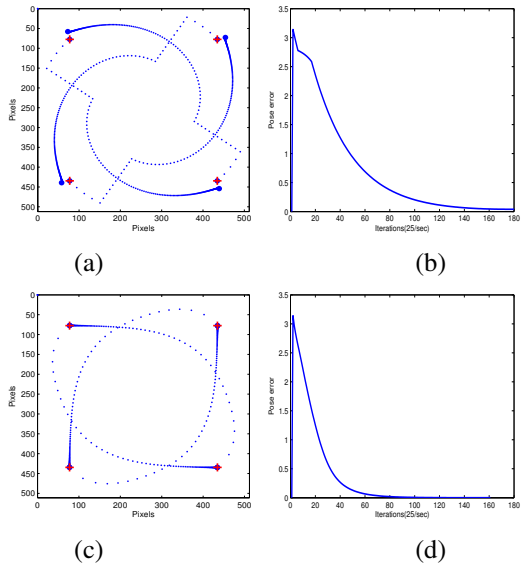


Fig. 3. The image features trajectories and pose error in presence of Cartesian local minima. Gans method in the first row and our integration method in the second row.

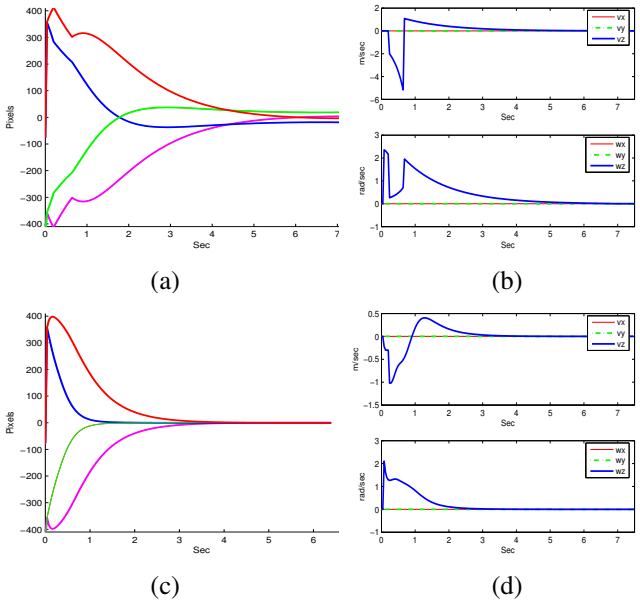


Fig. 4. The image error and velocity command in presence of Cartesian local minima. Gans method in the first row and our integration method in the second row.

the system avoids the local minima in the image and Cartesian spaces. In fact, the local minima in IBVS and PBVS are not correlated and do not tend to happen together. This justifies the claim that our method is globally asymptotically stable.

## VI. Simulation and Results

We present the simulation experiments where our proposed method is compared to the previous hybrid methods, namely switching methods proposed by Gans and Hutchinson [8], [13] and the one proposed by Chesi *et. al.* [9]. In the remaining of this paper and for comparison purpose, we call the first method as Gans' method and second one as Chesi's method. These two methods in addition to our proposed one are implemented.

The comparison is carried out for two positioning tasks. First one is with a 180 degrees rotation error around the camera optical axis. Using this task we will evaluate performance of the algorithm for keeping the visibility of features. The second task is a general positioning task that contains rotational and translational errors. The task is useful to evaluate the time of convergence and the continuity of the control signal. The servoing target object consists of four planar points. We assume a perspective projection camera model with unit aspect ratio. The processing rate is considered to be fixed at 25 frame/Sec.

### A. Feature-visibility and Local Minima

The positioning task with 180 degrees rotation error is used here. Our proposed method is compared to Gans' method and gave satisfactory results for the feature visibility as shown in Fig 3(a). Gans' method started with PBVS, producing a pure rotation about the camera optical axis. When the image features approach the image border, the control switches to IBVS, in order to keep the image features visibile. IBVS produces a straight line image trajectory but it is acompanied with a camera retreat in the Cartesian space. At the retreat threshold, the control switches back to PBVS to produce the pure rotation about the camera optical axis again. Where the image features stay far from the image border the control will continue with PBVS till the desired pose. Owing to errors in the pose estimation process, the system converges to a local minima in the nieghborhood of the desired pose. In Fig 3(a), the final position of the image features is a little diffirent from the desired one while the pose error in Fig 3(b) converges to a small value near to its zero dsired value. Figures 4(a) and 4(b) show the local minima where the velocity convergs to zero and the image error does not.

Our method successfully keeps the image features visibile, see Fig 3(c), during the servoing process. In the same figure one can see that the image features converge perfectly to the desired position depecting a global minima. The method also behaves perfectly with respect to the Cartesian local minima where the IBVS controller works to aviod the local minima while the output of PBVS controller is nullified. This is clear from the pose error in Fig 3(d). The image error and velocity command in Figs 4(c) and 4(d) converge both to zero that depicts a global minima.

### B. Discontinuity and Convergence Time

To evaluate the time of convergance and the smoothness of the velocity control signal, we use a general positioning task with both rotational and translational error. We compare it with both methods, Chesi's and Gans' one. Gans' method (Figs 5(a) and 5(b)) show a discontinuity in the control signal due to the switching between IBVS and PBVS. In Chesi's mehtod (Figs 5(c) and 5(d)), there are a frequent switching.

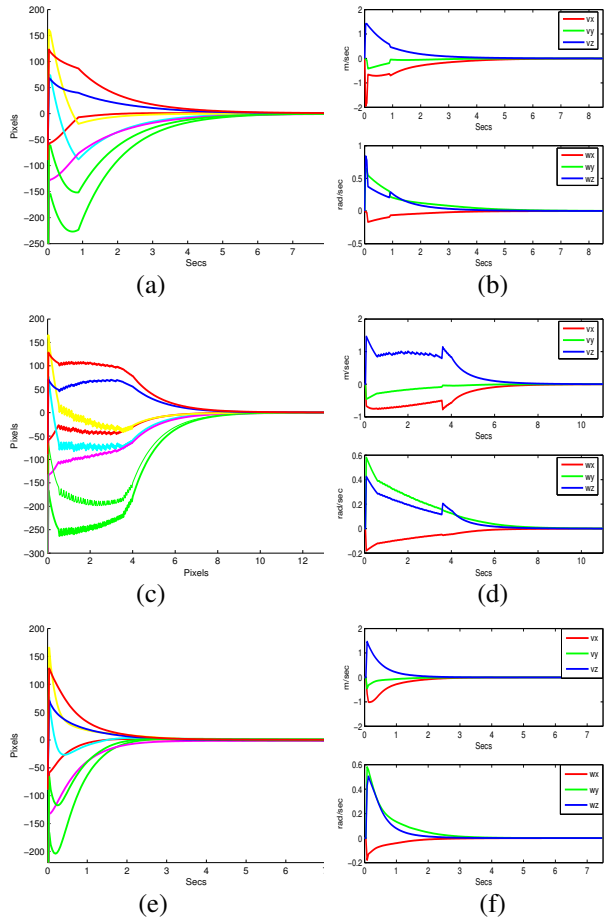


Fig. 5. The image error (left) and velocity command (right) show the discontinuity in Gans' method, (a) and (b), and Chesi's, (c) and (d). Our integration method shows faster convergence and smooth velocity command in (e) and (f).

This means a discontinuity in the control signal. In contrast to these two methods, our method (Figs 5(e) and 5(f)) provides a continuos and smooth control signal *i. e.* the velocity screw command.

The switching design of Gans' and Chesi's mehtods, in order to keep the visibility of the image features, came out with a delay in the convergence. This is clear from the image error graphs in Fig 5(a), 5(c), and 5(e). From the figures one can note that our integration method converges within 3-4 seconds, while Gans' method converges within 6-7 seconds and Chesi *et. al.* mehtod needs 9-10 seconds to converge for the same task.

## VII. Conclusion and Future Work

The method presented in this paper propose a unique solution that satisfies a set of widly addressed requirments in visual servoing literature. These requirments are such as feature visibility, local minima, and straight camera trajectory. The method gives similar performance to previous methods like Gans' one with respect to image features visibility. However, it gives faster convergance and continuous velocity control signal in contrast to the discontiuity present in other switching methods like Gans' and Chesi's ones. This method is a part of larger activity that aims to design a unified frame work to estimate the 3D information online. Then, use these information to improve the performance of visual servoing using this integration method.

## Acknowledgment

The authors would like to acknowledge Dr. F. Chaumette and Dr. E. Cervera for their valuable feedback on the early draft of this paper.

## References

[1] S. Hutchinson, G. Hager, and Cork, "A tutorial on visual servo control," *IEEE Transactions on Robotics and Automation*, vol. 17, pp. 18–27, 1996.

[2] E. Malis, F. Chaumette, and S. Boudet, "2 1/2 d visual servoing," *IEEE Transactions on Robotics and Automation*, vol. 15, no. 2, pp. 238–250, April 1999.

[3] P. Corck and S. Hutchinson, "A new partitioned approach to image-based visual servoing," *IEEE Transactions on Robotics and Automation*, vol. 14, no. 4, pp. 507–515, Aug 2001.

[4] F. Chaumette, "Potential problems of stability and convergence in image-based and position-based visual servoing," in *The Confluence of Vision and Control*, D. Kriegman, G. . Hager, and A. Morse, Eds. LNCIS Series, No 237, Springer-Verlag, 1998, pp. 66–78.

[5] L. Deng, F. Janabi-Sharifi, and W. J. Wilson, "Hybrid strategies for image constraints avoidance in visual servoing," in *IEEE/RSJ Int. Conf. on Intelligent Robots and Systems, IROS'02*, Switzerland, October 2002, pp. 348–353.

[6] Y. Mezouar and F. Chaumette, "Path planning for robust image-based control," *IEEE Trans. on Robotics and Automation*, vol. 18, no. 4, pp. 534–549, Aug 2002.

[7] O. Khatib, "Real time obstacle avoidance for manipulators and mobile robots," *International Journal of Robotics Research*, vol. 5, no. 1, pp. 90–98, 1986.

[8] N. R. Gans and S. A. Hutchinson, "An experimental study of hybrid switched system approach to visual servoing," in *IEEE Int. Conf. on Robotics and Automation, ICRA'03*, Taiwan, September 2003, pp. 3061–3068.

[9] G. Chesi, K. Hashimoto, D. Prattichizzo, and A. Vicino, "Keeping features in the field of view in eye-in-hand visual servoing: A switching approach," *IEEE Trans. on Robotics*, vol. 20, no. 5, pp. 534–549, Oct 2004.

[10] W. Wilson, C. C. W. Hulls, and G. S. Bell, "Relative endeffector control using cartesian position-based visual servoing," *IEEE Transactions on Robotics and Automation*, vol. 12, no. 5, pp. 684–696, October 1996.

[11] D. Leberzon and A. Stephen Morse, "Basic problems in stability and desgn of switched systems," *IEEE Control Systems Magazine*, pp. 59–70, October 1999.

[12] R. Shorten and K. Narendra, "On common quadratic lyapunov functions for pairs of stable lti systems whose system matrices are in companion form," *IEEE Transactions on Automatic Control*, vol. 48, no. 4, pp. 618–621, April 2003.

[13] N. R. Gans and S. A. Hutchinson, "An asymptotically stable switched system visual controller for eye in hand robots," in *IEEE/RSJ Int. Conf. on Intelligent Robots and Systems, IROS'03*, Las Vegas, October 2003, pp. 3061–3068.